

ScienceDirect



IFAC PapersOnLine 54-20 (2021) 310-315

Observer Design and Analysis for Non-Invasive Hemorrhage Detection

Xin Jin*, Yekanth Ram Chalumuri*, Ali Tivay*, Jin-Oh Hahn*

*University of Maryland, College Park, MD 20742 USA (Tel: 301-405-7864; e-mail: jhahn12@umd.edu)

Abstract: This paper presents the design and analysis of an observer to enable non-invasive hemorrhage detection. The proposed observer-based approach detects hemorrhage by continuously receiving the volume resuscitation inputted to a patient and the resulting hemoglobin response of the patient, and creating multiple state estimates as candidate signatures. A unique challenge differentiating the hemoglobin-based hemorrhage detection problem from conventional fault detection problems is that hemorrhage (i.e., the process fault) also alters the measurement equation. Through the design of an observer using a blood volume kinetics model as plant dynamics, and the extensive analysis of its error dynamics incorporating the process fault-induced alteration in sensing, it was demonstrated that hemorrhage can be detected based on the dynamic behaviors of the signatures generated by the observer: virtual in silico testing resulted in a F-score of 0.80 (precision: 0.91; recall: 0.78) and a normalized detection time of 0.1-0.7 relative to the time to 25% blood volume loss.

Copyright © 2021 The Authors. This is an open access article under the CC BY-NC-ND license (https://creativecommons.org/licenses/by-nc-nd/4.0/)

Keywords: observer, detection, fault, hemorrhage, hemoglobin.

1. INTRODUCTION

Hemorrhage is accountable for ~40% of mortality globally (Kauvar et al., 2006). Especially in combat casualty care, >85% of mortality on the battlefield is attributed primarily to hemorrhage, a quarter of which is survivable if timely treatment is provided (Eastridge et al., 2011). Hence, early detection of hemorrhage is of paramount importance in providing life-saving interventions to hemorrhaging patients. However, a chronic challenge is that traditional vital signs for patient monitoring (e.g., heart rate, blood pressure (BP), and oxygen saturation) may not reveal the symptoms of blood loss during early stages of hemorrhage due to the compensatory mechanisms in the body.

Effort to quickly detect hemorrhage and hemorrhage-induced circulatory decompensation has been made on algorithmic and sensing fronts. The algorithmic effort includes pulse wave analysis (PWA) (Nicia et al., 2016) and machine learningbased methods for detecting the depletion of blood volume (BV) (Reljin et al., 2018) as well as compensatory reserve (Convertino and Schiller, 2017). A potential limitation of the recently reported techniques is that they tend to be empiric and difficult to interpret due to their data-driven nature. addition, these techniques are often concerned with the assessment of margins to circulatory collapse rather than the detection of hemorrhage itself. The sensing effort includes, to list a few, continuous blood hemoglobin (Hgb) monitoring and ultrasound applications. Continuous Hgb monitoring via pulse co-oximetry (Frasca et al., 2011) and diffuse optical techniques (Vishwanath et al., 2018) showed promise despite plenty of room for innovations, while the ultrasound measurement of inferior vena cava diameter and left ventricle thickness was not responsive to hemorrhage (Resnick et al., 2011). Hence, there is a technological gap in early detection of hemorrhage both in algorithmic and sensing standpoints.

This paper presents the design and analysis of an observer to enable prompt and non-invasive hemorrhage detection. Our innovative idea is to leverage an interpretable mathematical model of BV kinetics (Bighamian et al., 2016) in conjunction with continuous Hgb measurement (SpHb, a widely used surrogate measure of BV expansion in response to volume resuscitation) to detect and assess hemorrhage. If the patient is subject to hemorrhage, the states in the BV kinetics model (with the assumption of no hemorrhage) will predict a SpHb response to volume resuscitation that has large discrepancy from the monitored SpHb. In this way, hemorrhage may be detected based on the relevancy of the behaviors associated with the states in the BV kinetics model, which are estimated by the observer as candidate signatures. A unique challenge differentiating the hemoglobin-based hemorrhage detection problem from conventional fault detection problems is that hemorrhage (i.e., the process fault) also alters the measurement equation. Through the design of an observer using a BV kinetics model as plant dynamics and the extensive analysis of its error dynamics incorporating the process fault-induced alteration in sensing, it was demonstrated that hemorrhage can be detected based on the dynamic behaviors of the signatures generated by the observer.

2. OBSERVER DESIGN AND ANALYSIS

2.1. Plant Dynamics: Blood Volume Kinetics

This work employed a lumped-parameter BV kinetics model developed in our prior work (Fig. 1) (Bighamian et al., 2017). The vast majority of mathematical models of BV kinetics developed to date (Tatara et al., 2007; Carlson et al., 1996; Gyenge et al., 2003; Kofránek and Rusz, 2010) intend to establish in-depth understanding of the BV kinetics itself and tend to include excessive details not observable in real clinical settings and thus not suited to observer design. In contrast, the lumped-parameter BV kinetics model retains the essential

high-level physiological principles (e.g., volume equilibrium and fluid shift) while lumping all the unnecessary details not suited to observer design into phenomenological models. The model is analogous to a two-bucket system, in which the intravascular and extravascular compartments are modeled as buckets, and the fluid shift as fluid flow through a valve connecting the buckets. It can be shown that the plant dynamics is written in the state-space representation in (1) (Bighamian et al., 2017):

$$\begin{bmatrix} \dot{x}_1 \\ \dot{x}_2 \end{bmatrix} = \begin{bmatrix} -k & 1 \\ 0 & 0 \end{bmatrix} \begin{bmatrix} x_1 \\ x_2 \end{bmatrix} + \begin{bmatrix} 1 \\ \frac{k}{1+\alpha_k} \end{bmatrix} u - \begin{bmatrix} 1 \\ \frac{k}{1+\alpha_k} \end{bmatrix} h \tag{1a}$$

$$y = \frac{1}{V_{B0}} x_1 = \frac{\sigma(0) - \sigma(t)}{\sigma(t)} - \frac{\int_0^t h(\tau) \sigma(\tau) d\tau}{V_{B0} \sigma(t)}$$
 (1b)

The model is characterized by four interpretable parameters: (i) pre-resuscitation/hemorrhage BV (V_{B0}) , (ii) volume split ratio α_u and α_h in the steady state, and (iii) fluid shift rate constant k. Fluid shift is modeled so that a $\frac{1}{1+\alpha_n}$ fraction of the inputted fluid is stored in the blood and the remaining $\frac{\alpha_u}{1+\alpha_u}$ fraction in the interstitial space. Likewise, a $\frac{\alpha_h}{1+\alpha_h}$ fraction of the blood lost is compensated by the interstitial space.

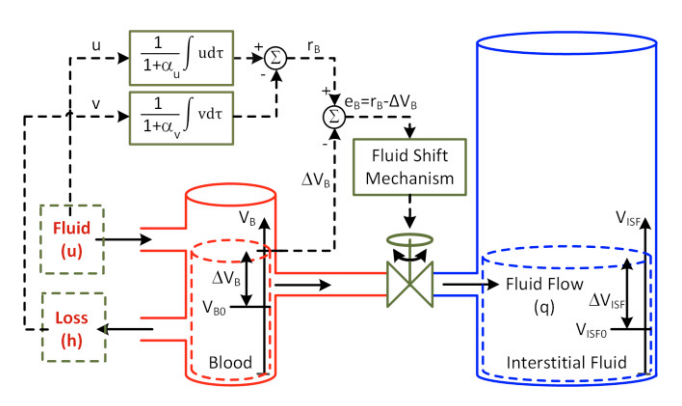


Fig. 1. Lumped-parameter blood volume kinetics model as the plant dynamics for observer design.

This work assumes that SpHb is available as measurement: $\sigma(t)$. In the absence of hemorrhage, $\frac{\sigma(0) - \sigma(t)}{\sigma(t)}$ is equal to the fractional BV change (Hahn, 2010). But, in the presence of hemorrhage, $\frac{\sigma(0) - \sigma(t)}{\sigma(t)}$ is equal to the fractional BV change plus an additional term related to the change in red blood cell (RBC) volume due to hemorrhage: $\frac{\int_0^t h(\tau)\sigma(\tau)d\tau}{V_{B0}\sigma(t)}$: $\frac{\sigma(0)-\sigma(t)}{\sigma(t)} =$ $\frac{\Delta V_B(t)}{V_{B0}} + \frac{\int_0^t h(\tau)\sigma(\tau)d\tau}{V_{B0}\sigma(t)}$ where ΔV_B is the change in BV from V_{B0} and h(t) is the hemorrhage rate. So, it is impossible to measure fractional BV change from SpHb in the presence of hemorrhage since h(t) is unknown.

2.2. Observer Design

Consider the following observer design model based on (1):

$$\dot{x} = Ax + Bu = \begin{bmatrix} -k & 1 & -1 \\ 0 & 0 & -\frac{k}{1+\alpha_h} \\ 0 & 0 & 0 \end{bmatrix} \begin{bmatrix} x_1 \\ x_2 \\ x_3 \end{bmatrix} + \begin{bmatrix} \frac{1}{k} \\ \frac{1+\alpha_u}{0} \end{bmatrix} u \quad (2)$$

where $A = \bar{A} + \tilde{A}$ and $B = \bar{B} + \tilde{B}$, with $\bar{\cdot}$ and $\tilde{\cdot}$ being nominal and uncertain parts, respectively. The measurement equation is given by:

$$z = \frac{1}{V_{R0}} x_1 = \frac{\sigma(0) - \sigma(t)}{\sigma(t)}$$
 (3)

 $z = \frac{1}{V_{B0}} x_1 = \frac{\sigma(0) - \sigma(t)}{\sigma(t)}$ where the unknown term $\frac{\int_0^t h(\tau) \sigma(\tau) d\tau}{V_{B0} \sigma(t)}$ in (1b) was neglected. Then, the Luenberger observer for (2) and (3) is given by:

$$\dot{\hat{x}} = \bar{A}\hat{x} + \bar{B}u + L\left[\left(\frac{1}{v_{B0}}x_1 + \frac{\int_0^t h(\tau)\sigma(\tau)d\tau}{v_{B0}\sigma(t)}\right) - \frac{1}{v_{B0}}\hat{x}_1\right]$$
 (4) where *L* is the observer gain that can be designed by, e.g., pole

placement.

2.3. Error Dynamics Analysis

Given (2)-(4), the error dynamics is given by:

$$\dot{e} = \dot{x} - \dot{\hat{x}}
= \bar{A}e - \frac{L}{V_{B0}} \begin{bmatrix} 1 & 0 & 0 \end{bmatrix} e + \tilde{A}x + \tilde{B}u - L \frac{\int_{0}^{t} h(\tau)\sigma(\tau)d\tau}{V_{B0}\sigma(t)}
= \left(\bar{A} - \frac{L}{V_{B0}} \begin{bmatrix} 1 & 0 & 0 \end{bmatrix}\right) e + w$$
(5)

where $w = \tilde{A}x + \tilde{B}u - L \frac{\int_0^t h(\tau)\sigma(\tau)d\tau}{V_{Po}\sigma(t)}$. Neglecting parametric uncertainty $(\tilde{A}x + \tilde{B}u = 0)$ to scrutinize the effect of h(t) on the errors and expanding (5) into component-wise equations:

$$\dot{e}_1 = -\left(k + \frac{l_1}{V_{Po}}\right)e_1 + e_2 - e_3 - l_1 w_h \tag{6a}$$

$$\dot{e}_2 = -\frac{l_2}{V_{R0}}e_1 - \frac{k}{1+\alpha_h}e_3 - l_2w_h \tag{6b}$$

the errors and expanding (5) into component-wise equations:

$$\dot{e}_1 = -\left(k + \frac{l_1}{V_{B0}}\right)e_1 + e_2 - e_3 - l_1w_h \tag{6a}$$

$$\dot{e}_2 = -\frac{l_2}{V_{B0}}e_1 - \frac{k}{1+\alpha_h}e_3 - l_2w_h \tag{6b}$$

$$\dot{e}_3 = -\frac{l_3}{V_{B0}}e_1 - l_3w_h \tag{6c}$$

where $w_h = \frac{\int_0^t h(\tau)\sigma(\tau)d\tau}{V_{B0}\sigma(t)} > 0$ is a monotonically increasing disturbance due to hemorrhage. In terms of transfer function:

$$e_{1}(s) = -\frac{l_{1}s^{2} + (l_{2} - l_{3})s - \frac{k}{1+\alpha_{h}}l_{3}}{s^{3} + \left(k + \frac{l_{1}}{V_{B0}}\right)s^{2} + \left(\frac{l_{2}}{V_{B0}} - \frac{l_{3}}{V_{B0}}\right)s - \frac{k}{1+\alpha_{h}}V_{B0}} w_{h}(s)$$
(7a)
$$e_{2}(s) = -\frac{l_{2}s^{2} + \left(kl_{2} - \frac{k}{1+\alpha_{h}}l_{3}\right)s - \frac{k^{2}}{1+\alpha_{h}}l_{3}}{s^{3} + \left(k + \frac{l_{1}}{V_{B0}}\right)s^{2} + \left(\frac{l_{2}}{V_{B0}} - \frac{l_{3}}{V_{B0}}\right)s - \frac{k}{1+\alpha_{h}}V_{B0}} w_{h}(s)$$
(7b)
$$e_{3}(s) = -\frac{l_{3}s^{2} + kl_{3}s}{s^{3} + \left(k + \frac{l_{1}}{V_{B0}}\right)s^{2} + \left(\frac{l_{2}}{V_{B0}} - \frac{l_{3}}{V_{B0}}\right)s - \frac{k}{1+\alpha_{h}}V_{B0}} w_{h}(s)$$
(7c)

$$e_2(s) = -\frac{l_2 s^2 + \left(k l_2 - \frac{k}{1 + \alpha_h} l_3\right) s - \frac{k^2}{1 + \alpha_h} l_3}{s^3 + \left(k + \frac{l_1}{V_{RO}}\right) s^2 + \left(\frac{l_2}{V_{RO}} - \frac{l_3}{V_{RO}}\right) s - \frac{k}{1 + \alpha_h V_{RO}}} w_h(s)$$
(7b)

$$e_3(s) = -\frac{l_3 s^2 + k l_3 s}{s^3 + \left(k + \frac{l_1}{V_{B0}}\right) s^2 + \left(\frac{l_2}{V_{B0}} - \frac{l_3}{V_{B0}}\right) s - \frac{k}{1 + \alpha_h V_{B0}}} w_h(s) \tag{7c}$$

where $\dot{w}_h = \frac{d}{dt} \left[\frac{\int_0^t h(\tau) \sigma(\tau) d\tau}{V_{B0} \sigma(t)} \right] = \frac{1}{V_{B0}} \left(h - \frac{\dot{\sigma} \int_0^t h(\tau) \sigma(\tau) d\tau}{\sigma^2} \right) \ge \frac{h}{V_{B0}}$ since $h \ge 0$, $\sigma \ge 0$ (since SpHb is positive), and $\dot{\sigma} \le 0$ (since SpHb decrease under hemorrhage). Hence, $w_h \ge \frac{\int_0^t h(\tau)d\tau}{V_{B0}}$. If h(t) is assumed to be slowly varying and is approximated to a step signal (i.e., $h(s) \approx \frac{H}{s}$), then $w_h(s) \ge \frac{H}{v_{B0}s^2}$. Therefore, $\lim_{t\to\infty}e_1(t)=\infty, \lim_{t\to\infty}e_2(t)=\infty, \text{ and } \lim_{t\to\infty}e_3(t)\geq (1+\alpha_h)H,$ and in addition, $\lim_{t\to\infty}\dot{e}_1(t)\leq -H \text{ and } \lim_{t\to\infty}\dot{e}_2(t)\leq -kH. \text{ In }$ sum, assuming that h(t) is slowly varying, hemorrhage can be detected if any of the following conditions is satisfied:

- 1) C1: $\lim_{t\to\infty}e_1(t)\leq -H\to \hat{x}_1(t)>\bar{x}_1(t)$, with $\bar{x}_1(t)$ being the upper bound of $x_1(t)$ in (2), i.e., when $h(t)=0, \forall t\geq 0$.
- 2) C2: $\lim_{t\to\infty} \dot{e}_1(t) \leq -H \to \dot{\hat{x}}_1(t) > \dot{\bar{x}}_1(t)$, with $\dot{\bar{x}}_1(t)$ being the upper bound of $\dot{x}_1(t)$ in (2), i.e., when $h(t) = 0, \forall t \geq 0$.
- 3) C3: $\lim_{t\to\infty} \dot{e}_2(t) \leq -kH \to \dot{\hat{x}}_2(t) > \dot{\bar{x}}_2(t)$, with $\dot{\bar{x}}_2(t)$ being the upper bound of $\dot{x}_2(t)$ in (2), i.e., when $h(t)=0, \forall t\geq 0$.
- 4) C4: $\lim_{t\to\infty} e_3(t) \ge (1+\alpha_h)H \to \hat{x}_3(t) < \underline{x}_3(t)$, with $\underline{x}_3(t)$ being the lower bound of $x_3(t)$ in (2), i.e., when h(t) = 0, $\forall t \ge 0$.

2.3. Virtual In Silico Testing and Data Analysis

To conduct extensive virtual in silico testing of the observer-based approach to hemorrhage detection, virtual patients were created using (1) in conjunction with a dataset acquired from 23 sheep subjects undergoing acute hemorrhage and volume resuscitation and a novel collective Bayesian inference-based generative modeling framework developed based on our prior work (A Tivay et al., 2020; A. Tivay et al., 2020). In brief, each sheep was subjected to a large initial (25ml/kg) and two subsequent small hemorrhages (5ml/kg). Each sheep received volume resuscitation with the Ringer's Lactate by closed-loop control algorithms designed to restore and maintain mean BP. Details of the dataset and the control algorithms are provided elsewhere (Marques et al., 2017; Rafie et al., 2004; Vaid et al., 2006). A total of 200 realistic virtual patients were created and employed in our virtual in silico testing.

In each virtual patient, the hemorrhage detection performance was examined under a wide range of hemorrhage (0.025ml/kg/min - 1.15ml/kg/min) and volume resuscitation (0ml/kg to the hemorrhage rate under consideration) rates. To make the virtual test more realistic, the SpHb signal outputted by the virtual patient was corrupted by a white noise of 5%. For each hemorrhage and resuscitation rate pair in each virtual patient, we also considered the corresponding zero hemorrhage rate scenario in which the virtual patient received only volume resuscitation in the absence of blood loss. In this way, the efficacy of the approach in making true detection and avoiding false detection could be evaluated.

For each hemorrhage and resuscitation rate pair in each virtual patient, hemorrhage detection was performed as follows. The observer (4) generated state estimates \hat{x}_1 , $\dot{\hat{x}}_1$, $\dot{\hat{x}}_2$, and \hat{x}_3 based on the volume resuscitation input and SpHb response, while the plant dynamics (2) was solved concurrently for a large number of virtual patients to determine the bounds $\bar{x}_1(t)$ as well as $\dot{\bar{x}}_1(t)$, $\dot{\bar{x}}_2(t)$ and $\bar{x}_3(t)$ in response to the given volume resuscitation on the fly. These bounds were selected to cover 90% of all the virtual patient responses. The observer-based estimates were then filtered via 20-point averaging to mitigate the effect of measurement noise. At each sampling instant, the conditions described in Section 2.2 were evaluated in a causal moving time interval of a pre-specified duration (15 min to the past in this work) using all the samples therein (15 samples with a sampling rate of 0.016 Hz in this work). For a given

detection condition, hemorrhage was detected if (i) the probability of satisfying the condition in the moving time interval was higher than a pre-specified threshold value (80 %) for longer than a pre-specified duration (15 min in this work) and (ii) hemorrhage was detected before a pre-specified volume of blood was lost (25% in this work). The rationale underlying these criteria was to (i) mitigate the adverse effect of measurement noise (which may result in isolated samples invalidating the conditions) and (ii) discard practically meaningless detection (patient may not be resuscitated if hemorrhage is detected after a large volume of blood is lost).

The hemorrhage detection performance of the four conditions in Section 2.2 was evaluated individually. For each condition, we computed precision, recall, and F-score using the outcomes of hemorrhage detection associated with all the hemorrhage and volume resuscitation rate pairs as representative metrics of performance. We also computed the same metrics associated with each hemorrhage and volume resuscitation rate pair. To scrutinize how quickly hemorrhage is detected in case of true positive outcomes, we computed the "normalized detection time," defined as the time hemorrhage is detected divided by the time corresponding to the loss of a pre-specified BV (25 % in this work), both with reference to the time of hemorrhage onset). The normalized detection time was computed using (i) the true positive hemorrhage detection outcomes associated with all the hemorrhage and volume resuscitation rate pairs as representative metric of performance as well as (ii) the true positive hemorrhage detection outcomes associated with each hemorrhage and volume resuscitation rate pair.

3. RESULTS AND DISCUSSION

Table 1 shows the performance of observer-based hemorrhage detection in terms of precision, recall, F-score, and normalized detection time while Table 2 shows the performance of observer-based hemorrhage detection in terms of F-score at slow, moderate, and fast hemorrhage. Fig. 2 shows precision, recall, F-score across hemorrhage and resuscitation rates. Fig. 3 shows the average normalized detection time across hemorrhage and resuscitation rates, while Fig. 4 shows its actual distribution associated with (a) low, (b) moderate, and (c) high hemorrhage rates.

Table 1. Efficacy of observer-based hemorrhage detection.

Condition	Precision	Recall	F-Score	NDT
1	0.31	0.39	0.34	0.65
2	0.88	0.70	0.72	0.42
3	0.76	0.34	0.44	0.40
4	0.91	0.78	0.80	0.45

In general, C2 and C4 outperformed C1 and C3 in F-score as well as precision and recall. C4 appeared to perform the best all in all. In terms of NDT, C2, C3, and C4 were comparable while C1 largely underperformed. Scrutinizing Fig. 2 provides deeper insight regarding why C2 and C4 are superior to C1 and C3. C1 and C3 are effective only under low hemorrhage rates and/or high resuscitation rates (I/H ratio: the ratio between the

(c)

resuscitation rate and the hemorrhage rate). In contrast, C2 and C4 exhibit satisfactory performance across a wide range of hemorrhage and resuscitation rates. These trends were commonly observed for precision, recall, and F-score.

Table 2. Efficacy of observer-based hemorrhage detection in relation to hemorrhage rates. P: precision. R: recall. F: F-score.

С	ondition	Slow	Moderate	Fast
1	P	0.62	0.27	0.16
	R	0.91	0.31	0.18
	F	0.74	0.29	0.17
2	P	0.93	0.96	0.69
	R	0.99	0.84	0.36
	F	0.96	0.88	0.41
3	P	0.93	0.77	0.60
	R	0.80	0.34	0.20
	F	0.84	0.41	0.25
4	P	0.89	0.97	0.77
	R	0.99	0.92	0.47
	F	0.94	0.94	0.53

It was of interest to garner in-depth insight on the mechanisms underlying the relationship of precision, recall, and F-score to hemorrhage and resuscitation rates. Fig. 2 indicates that the efficacy of all the conditions tends to degrade as hemorrhage rate increases and resuscitation rate decreases. This may be attributed to (i) the impact of hemorrhage and resuscitation rates on BV and (ii) uncertainty acting as disturbance to the observer. First, BV decreases faster when (i) hemorrhage rate is high and (ii) resuscitation rate is low. Hence, the time to loss of 25% BV is small under these conditions, which reduces the chance of detecting hemorrhage promptly before 25% BV is lost, thus decreasing true positives (and degrading precision and F-score) while increasing false negatives (and degrading recall and F-score). Indeed, F-score was high under slow hemorrhage but low under fast hemorrhage. Under high hemorrhage rates, the efficacy of observer-based hemorrhage detection was only marginal. Second, the uncertainty due to inter-individual variability exceeding the detection thresholds $\bar{x}_1(t), \dot{\bar{x}}_1(t), \dot{\bar{x}}_2(t),$ and $x_3(t)$ as well as measurement noise triggered false alarms, thereby decreasing true negatives while increasing false positives (and degrading precision).

In general, NDT associated with all the conditions degraded as hemorrhage rate increased and resuscitation rate decreased. Similarly to the hemorrhage detection metrics, this is attributed at least in part to the impact of hemorrhage and resuscitation rates on BV: BV decreases faster when (i) hemorrhage fast and (ii) resuscitation is slow. Hence, the time to loss of 25% BV is small under these conditions, which ends up with increasing NDT. Notably, NDT was small under fast hemorrhage and slow resuscitation in C2, C3, and C4. But, the NDT in this region was associated with very small number of true positive cases, and hemorrhage was not detected in most virtual patients (i.e., most virtual patients were associated with false negatives). In fact, NDT pertaining to C2 and C4 exhibited a (roughly) decreasing trend as I/H ratio increased in slow and moderate hemorrhage (in which F-score was high).

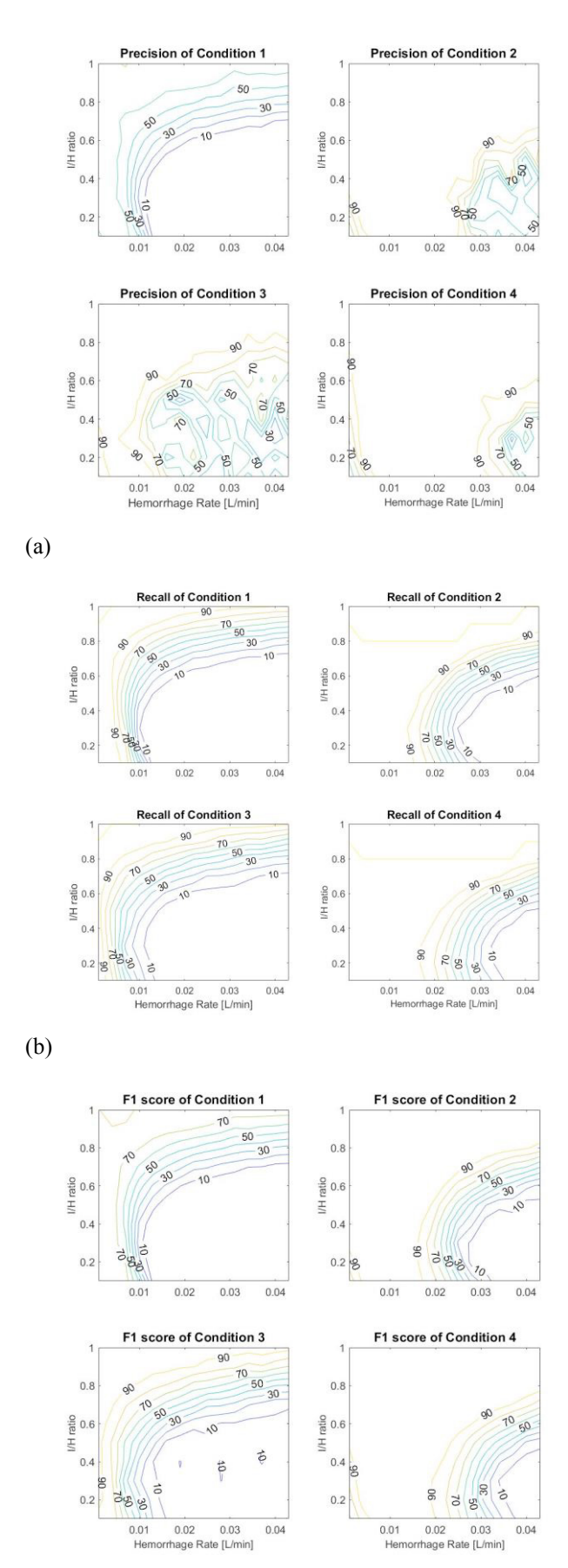


Fig. 2. Efficacy of observer-based hemorrhage detection with respect to hemorrhage and volume resuscitation rates.

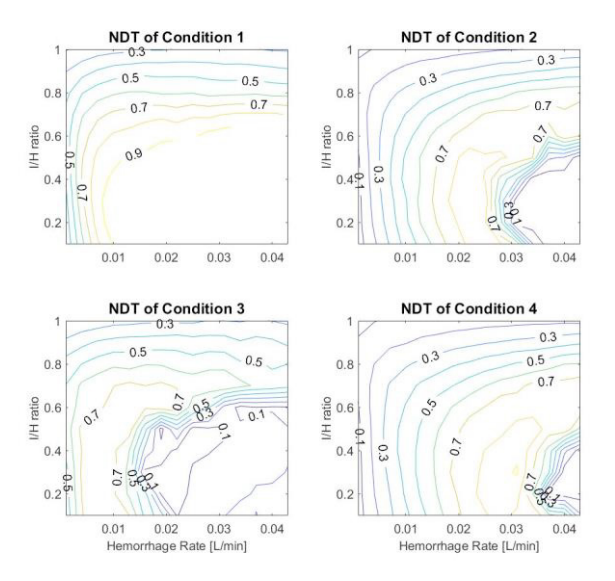


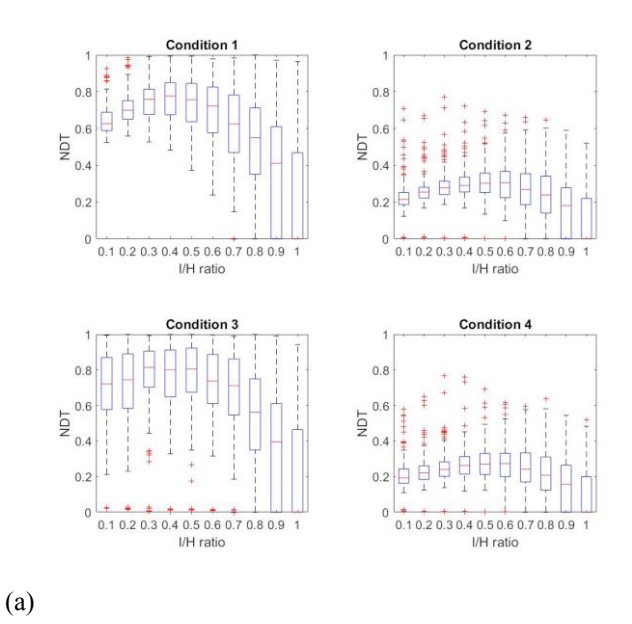
Fig. 3. Average normalized detection time across hemorrhage and resuscitation rates.

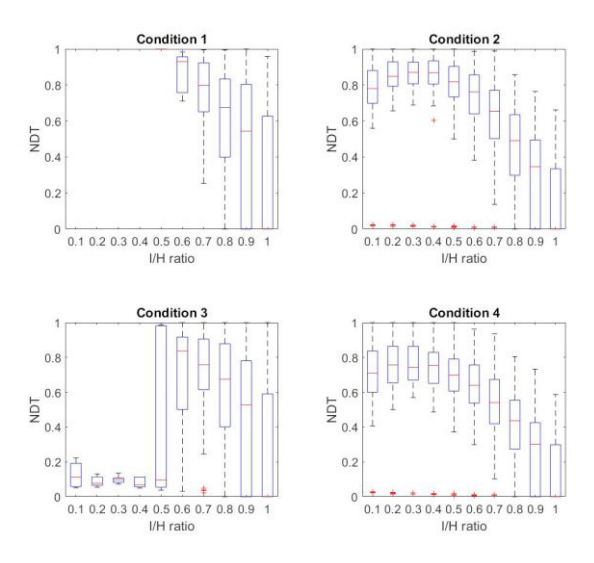
4. CONCLUSIONS

The feasibility of non-invasive hemorrhage detection based on readily available SpHb measurements was investigated. It was demonstrated that hemorrhage detection may be feasible with the integration of a lumped-parameter BV kinetics model and an observer in conjunction with real-time Hgb measurement. The observer-based hemorrhage detection approach exhibited promising performance under a wide range of hemorrhage and resuscitation rates, although its efficacy degraded under fast hemorrhage and/or slow resuscitation. Future work includes optimization of the observer-based approach, development of alternative approaches (including parameter estimation-based approach), and judicious fusion of detection conditions to enable more accurate and robust hemorrhage detection.

ACKNOWLEDGEMENT

This work was supported in part by the U.S. National Science Foundation under grants CMMI-1760817 and CNS-1748762.





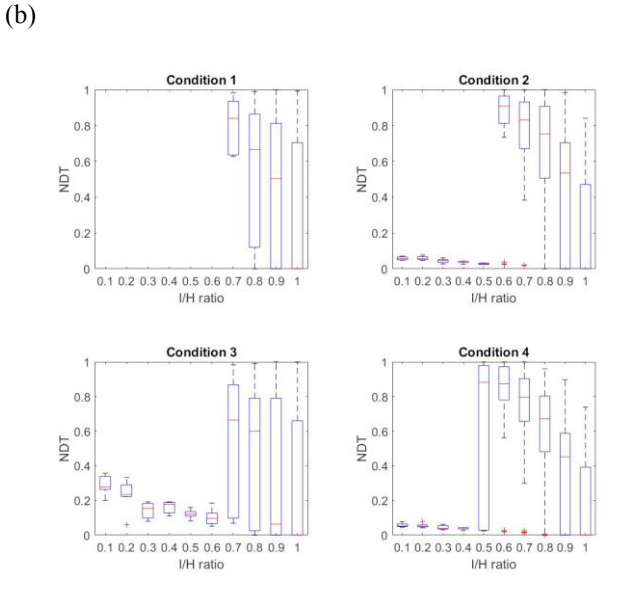


Fig. 4. Normalized detection time associated with (a) low, (b) moderate, and (c) high hemorrhage rates.

REFERENCES

- Bighamian, R., Kinsky, M., Kramer, G., Hahn, J.-O., 2017. In-Human Subject-Specific Evaluation of a Control-Theoretic Plasma Volume Regulation Model. Comput. Biol. Med. 91, 96–102. https://doi.org/10.1016/i.compbiomed.2017.10.006
- Bighamian, R., Reisner, A.T., Hahn, J.O., 2016. A lumped-parameter subject-specific model of blood volume response to fluid infusion. Front. Physiol. 7, 1–11. https://doi.org/10.3389/fphys.2016.00390
- Carlson, D.E., Kligman, M.D., Gann, D.S., 1996. Impairment of blood volume restitution after large hemorrhage: a mathematical model. Am. J. Physiol. 270, R1163–R1177.
- Convertino, V.A., Schiller, A.M., 2017. Measuring the Compensatory Reserve to Identify Shock. J. Trauma Acute Care Surg. 82, S57–S65. https://doi.org/10.1097/ta.0000000000001430
- Eastridge, B.J., Hardin, M., Cantrell, J., Oetjen-Gerdes, L.,
 Zubko, T., Mallak, C., Wade, C.E., Simmons, J., Mace,
 J., Mabry, R., Bolenbaucher, R., Blackbourne, L.H.,
 2011. Died of Wounds on the Battlefield: Causation and
 Implications for Improving Combat Casualty Care. J.
 Trauma 71, S4–S8.
- Frasca, D., Dahyot-Fizelier, C., Catherine, K., Levrat, Q., Debaene, B., Mimoz, O., 2011. Accuracy of a Continuous Noninvasive Hemoglobin Monitor in Intensive Care Unit Patients. Crit. Care Med. 39, 2277–2282. https://doi.org/10.1097/CCM.0b013e3182227e2d
- Gyenge, C.C., Bowen, B.D., Reed, R.K., Bert, J.L., 2003. Preliminary model of fluid and solute distribution and transport during hemorrhage. Ann. Biomed. Eng. 31, 823–839. https://doi.org/10.1114/1.1581878
- Hahn, R.G., 2010. Volume Kinetics for Infusion Fluids. Anesthesiology 113, 470–481.
- Kauvar, D.S., Lefering, R., Wade, C.E., 2006. Impact of Hemorrhage on Trauma Outcome: An Overview of Epidemiology, Clinical Presentations, and Therapeutic Considerations. J. Trauma 60, S3-11. https://doi.org/10.1097/01.ta.0000199961.02677.19
- Kofránek, J., Rusz, J., 2010. Restoration of Guyton's diagram for regulation of the circulation as a basis for quantitative physiological model development. Physiol. Res. 59, 897–908. https://doi.org/931838 [pii]
- Marques, N.R., Ford, B.J., Khan, M.N., Kinsky, M., Deyo,
 D.J., Mileski, W.J., Ying, H., Kramer, G.C., 2017.
 Automated Closed-Loop Resuscitation of Multiple Hemorrhages: A Comparison between Fuzzy Logic and Decision Table Controllers in a Sheep Model. Disaster Mil. Med. 3, 1. https://doi.org/10.1186/s40696-016-0029-0
- Nicia, S.B., Van Veelen, T.A., Stens, J., Koopman, M.M.W., Boer, C., 2016. Detection of Volume Loss Using the Nexfin Device in Blood Donors. Anaesthesia 71, 163–170. https://doi.org/10.1111/anae.13283
- Rafie, A.D., Rath, P.A., Michell, M.W., Kirschner, R.A., Deyo, D.J., Prough, D.S., Grady, J.J., Kramer, G.C.,

- 2004. Hypotensive resuscitation of multiple hemorrhages using crystalloid and colloids. Shock 22, 262–269.
- https://doi.org/10.1097/01.shk.0000135255.59817.8c
- Reljin, N., Zimmer, G., Malyuta, Y., Shelley, K., Mendelson, Y., Blehar, D.J., Darling, C.E., Chon, K.H., 2018. Using Support Vector Machines on Photoplethysmographic Signals to Discriminate between Hypovolemia and Euvolemia. PLoS One 13, e0195087. https://doi.org/http://dx.doi.org/10.1371/journal.pone.0 195087
- Resnick, J., Cydulka, R., Platz, E., Jones, R., 2011. Ultrasound Does Not Detect Early Blood Loss in Healthy Volunteers Donating Blood. J. Emerg. Med. 41, 270–275. https://doi.org/10.1016/j.jemermed.2010.11.040
- Tatara, T., Tsunetoh, T., Tashiro, C., 2007. Crystalloid infusion rate during fluid resuscitation from acute haemorrhage. Br. J. Anaesth. 99, 212–217. https://doi.org/10.1093/bja/aem165
- Tivay, A, Jin, X., Lo, A., Scully, C.G., Hahn, J.-O., 2020. Practical Use of Regularization in Individualizing a Mathematical Model of Cardiovascular Hemodynamics Using Scarce Data. Front. Physiol. 11, Article 452. https://doi.org/10.3389/fphys.2020.00452
- Tivay, A., Kramer, G.C., Hahn, J.-O., 2020. Virtual Patient Generation using Physiological Models through a Compressed Latent Parameterization, in: Proceedings of the American Control Conference. https://doi.org/10.23919/ACC45564.2020.9147298
- Vaid, S.U., Shah, A., Michell, M.W., Rafie, A.D., Deyo, D.J., Prough, D.S., Kramer, G.C., 2006. Normotensive and hypotensive closed-loop resuscitation using 3.0% NaCl to treat multiple hemorrhages in sheep. Crit. Care Med. 34, 1185–1192. https://doi.org/10.1097/01.CCM.0000207341.78696.3A
- Vishwanath, K., Gurjar, R., Wolf, D., Riccardi, S., Duggan, M., King, D., 2018. Diffuse Optical Monitoring of Peripheral Tissues During Uncontrolled Internal Hemorrhage in a Porcine Model. Biomed. Opt. Express 9, 569. https://doi.org/10.1364/boe.9.000569